

bandwidth-tunable range of 0.32 nm to 0.8 nm. According to the previous analysis, the bandwidth BW_0 of the drop transmission of a single add/drop MRR should be about 0.32 nm. A silicon-on-insulator (SOI) wafer with top silicon layer of 250 nm is selected for the design. The design radius R of the MRR is 10 μm . The cross section of the waveguide is designed as illustrated in Fig. 4(a). The waveguide width and height are designed to be 430 nm and 250 nm, respectively. A layer of benzocyclobutene (BCB) is used to cover the waveguide and form the upper cladding layer. A 100 nm Ti with 5 nm Au heater is deposited on top of the BCB for thermal tuning. To minimize the crosstalk between TE and TM modes, the device is designed for TM mode operation (Fig. 4(b)), since the coupling for the TE mode is much smaller in our design. By extending the 2D planar waveguide model [14] to 3D waveguide structures [15], the scattering loss is evaluated to be 3.1 dB/cm when calculated using the mode profile (Fig. 4(b)) associated with typical sidewall roughness standard deviation σ of 3 nm and its correlation length L_c of 50 nm [16] for the designed waveguide structure. Considering the relationship between BW_0 and $|\kappa|^2$ according to $BW_0 = 2|\kappa|^2 \lambda^2 / [(2\pi)^2 R n_{eff}]$ [17], n_{eff} being the effective index of the designed waveguide, a bandwidth BW_0 of 0.32 nm is obtained for a single add/drop MRR, provided the power coupling coefficient $|\kappa|^2$ is equal to 5.2%, corresponding to a coupling gap of 410 nm (calculated by the coupled mode theory according to [18,19]).

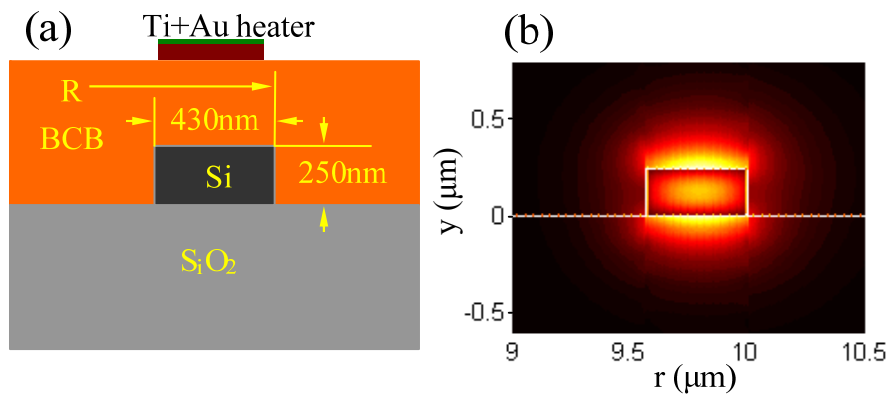


Fig. 4. (a) Cross section of the designed waveguide and (b) corresponding TM_0 mode profile of the electric field calculated by the full vectorial mode matching method [20,21].

Figure 5 shows pictures of the fabricated device. The device is fabricated on a SOI wafer with top silicon thickness of 250 nm and buried silicon dioxide of 3 μm . Diluted (1:1 in anisole) electron-beam resist ZEP520A is spin-coated on the wafer to form a ~ 110 nm-thick mask layer. The microring-MZI structure is then defined using electron-beam lithography (JEOL JBX-9300FS). After that, the sample is etched by inductively coupled plasma reactive ion etching (ICP-RIE) to transfer the patterns to the top silicon layer. Afterwards, a top cladding layer of 550 nm BCB is spin-coated for planarization, and a layer of 400 nm ZEP520A is spin-coated in sequence as the mask layer for the heaters. Electron-beam lithography is used again to define the patterns of the heaters and pads. Finally, heaters and pads (100 nm thick titanium with 5 nm thick Au) are formed by evaporation and lift-off techniques. The radii of the two MRRs are 10 μm , with waveguide width of 435 nm and coupling gap of 402 nm for both through and drop coupling regions, as shown in Fig. 5(a).

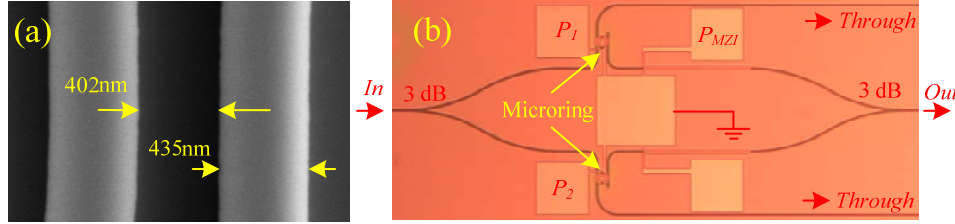


Fig. 5. (a) Scanning electron microscope (SEM) top view image of the coupling region of the MRR. (b) Optical microscope picture of the fabricated device. Two identical add-drop MRRs with micro-heaters are inserted in the two arms of the MZI structure. Heating powers of P_1 and P_2 , are applied to the MRR heaters, while a heating power of P_{MZI} is applied to one of the heaters deposited on top of the straight sections of the MZI.

4. Experimental results

4.1 SF and ER improvement

Figure 6(a) shows the measured through transmission of a single MRR at the through port, as shown in Fig. 5(b). Note that the transmission is normalized to that of a straight waveguide with the same cross section. Around 3.6 dB insertion loss is obtained because of the 3 dB splitter as shown in Fig. 5(b). By fitting the measured through transmission, a power coupling coefficient of 5.5% is obtained, which agrees well with the design. However, a fitted roundtrip field transmission coefficient a of 0.92 (corresponding to a propagation loss of 120 dB/cm) is obtained, which deviates significantly from the estimated scattering loss. This is potentially due to the excess loss induced by the metal heater. From Fig. 4(b), one can find that the field distribution of the TM_0 mode of the designed waveguide extends beyond 600 nm above the waveguide in the upper cladding layer. Since the top cladding layer is only 550 nm thick, the field overlaps with the metal heater, leading to a large propagation loss. Figure 6(b) shows the measured transmissions for the TM mode of the fabricated device. When $\phi_{MZI} = 0$ ($P_{MZI} = 0$ mW), the transmission of the device almost has a Lorentzian-shape with low ER. Using the fitted power coupling coefficient and a from Fig. 6(a), the calculated filter response shows good agreement with the measured transmission, as shown in Fig. 6(b). As predicted in the previous analysis, when $\phi_{MZI} = \pi$ ($P_{MZI} = 11.6$ mW), the ER is greatly improved to 30 dB. Moreover, the SF is also significantly improved to a value of 0.43, with -1 dB and -10 dB bandwidths of 0.52 nm and 1.2 nm, respectively. An insertion loss of 15 dB is measured, which is due to the large propagation loss as analyzed before. However, the insertion loss can be greatly improved using a thicker top cladding layer in order to reduce the propagation loss induced by the metal heater.

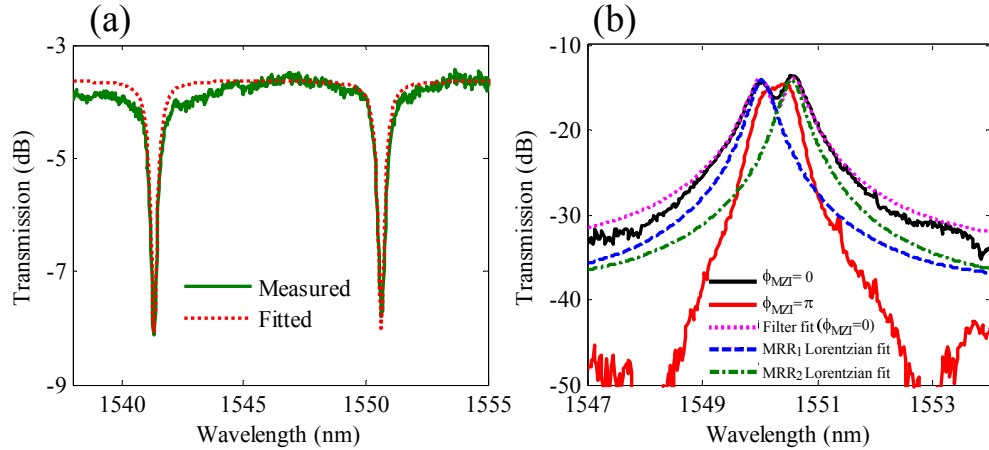


Fig. 6. (a) Measured and fitted through transmission, which is normalized to a straight waveguide, of a single MRR. (b) Measured transfer functions showing SF and ER improvement at $\phi_{MZI} = \pi$ ($P_{MZI} = 11.6$ mW) compared to the Lorentzian-shapes at $\phi_{MZI} = 0$ ($P_{MZI} = 0$ mW). Lorentzian fits of the transmissions of the two MRRs, as well as the filter are also represented.

4.2 Bandwidth tunability

Figure 7 shows the measured 3 dB bandwidth tunability (for an in-band ripple smaller than 1 dB) of the fabricated device working on TM mode. The heating power of the MZI arm is kept to 11.6 mW to maintain a π phase difference between the two MZI arms. Both P_1 and P_2 are adjusted to preserve the centre wavelength. One can find that, by applying different heating powers to the two MRRs, the resonance offset is effectively tuned, resulting in tuning of the bandwidth, as shown in Fig. 7(a). The 3 dB bandwidth can be linearly tuned by P_1 from 0.46 nm to 0.88 nm, which almost agrees with the design, as illustrated in Fig. 7(b). About 30 dB ER is obtained. The SF increases with increasing bandwidth, which also agrees with the simulations. However, a drop of the SF for $P_1 = 0.88$ mW and $P_2 = 4.14$ mW is observed, which is deteriorated by the imperfect splitting ratio of the 3 dB splitter.

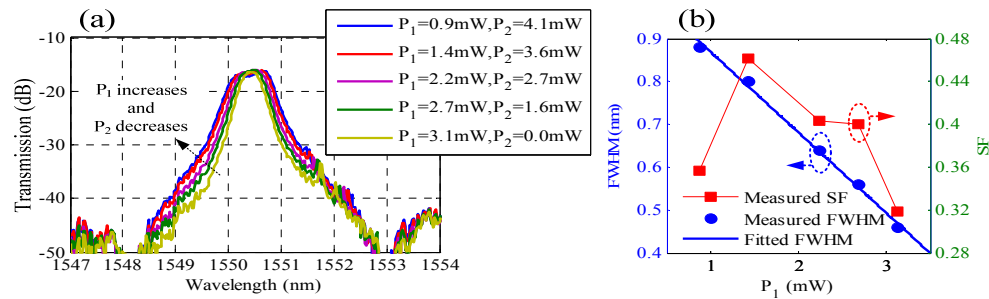


Fig. 7. (a) Measured bandwidth tunability of the fabricated device for in-band ripple smaller than 1 dB. The straight waveguide heating power is $P_{MZI} = 11.6$ mW. (b) FWHM bandwidth and shape factor of the filter as a function of the heating power applied to one of the MRRs.

4.3 Wavelength tunability

Figure 8 represents the wavelength tunability (for in-band ripple smaller than 1 dB) of the fabricated device working on TM mode. The heating power of the MZI arm is still 11.6 mW to keep a π phase difference between the two MZI arms. Both P_1 and P_2 are adjusted so that the shape of the filter keeps unchanged during the wavelength tuning. As shown in Fig. 8(a),

the center wavelength of the passband is tuned by tuning the heating powers applied to the two MRRs. The center wavelength evolution as a function of the heating power P_1 , which can be seen to be linear from 1550 to 1554 nm, is represented in Fig. 8(b). The wavelength tunability can be further improved by using SiO₂ or hydrogen silsesquioxane (HSQ) as the top cladding layer instead of BCB, due to their better thermal conductivity. The SF is also monitored during the wavelength tuning. One can find that the SF can be kept around 0.33~0.5, without notable degradation during the wavelength tuning. Due to the imperfect TE mode extinction of the polarization controller, there remains some residual TE mode light. Such TE crosstalk can be released by introducing a polarizer, for instance a photonic crystal, after the microring-MZI to block the TE mode light [22].

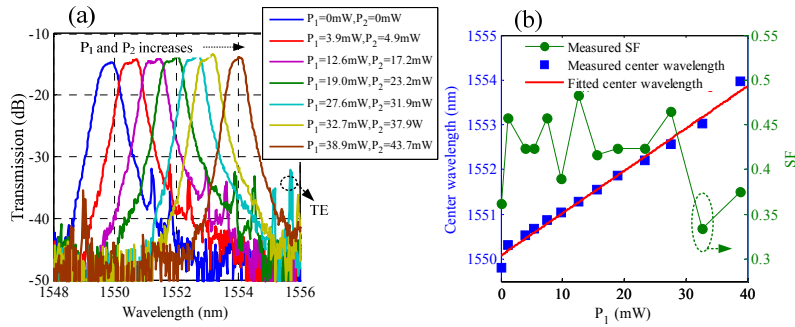


Fig. 8. (a) Transmission of the device for different heating powers combinations applied to the two MRRs, showing the center wavelength tunability. (b) Evolution of the center wavelength of the passband as a function of heating powers, as well as SF measured when tuning the wavelength. Only transfer functions with in-band ripple smaller than 1 dB are considered. The straight arm heating power is $P_{MZI} = 11.6\text{mW}$.

5. Conclusion

We have proposed and demonstrated a bandwidth and wavelength-tunable OBPF based on a silicon microring-MZI structure. An effective bandwidth tuning range from 0.46 to 0.88 nm, and wavelength tuning range from 1550 to 1554 nm are demonstrated experimentally with proper adjustment of the heating powers applied to the two MRRs and the straight section of the MZI. Good ER and SF are also obtained for the device. Due to its CMOS-compatible fabrication process, compact size, good ER and SF performances, and flexible bandwidth and wavelength tunability, our scheme is very promising for practical implementations.

Acknowledgments

This research was sponsored by the National Natural Science Foundation of China (Grant No. 60577007), and the National Basic Research Program of China (Grant No. 2006CB302805). Yunhong Ding would like to thank the Chinese Scholar Council (CSC) for the support. Yunhong Ding also acknowledges Kresten Yvind and David Larsson for the supply of the probe station. Supports from the Villum Kann Rasmussen foundation through the Nanophotonics for Terabit Communications (NATEC) centre of excellence, and National Natural Science Foundation of China (Grant No.60867002) are also acknowledged.